Frequency chirp effects on stimulated Raman scattering in inhomogeneous plasmas

Mufei Luo, Stefan Hüller, Min Chen, Zhengming Sheng

Frequency chirp effects on stimulated Raman scattering in inhomogeneous plasmas

Mufei Luo,[1,2,3,a)] Stefan Hüller,[3] Min Chen,[1,2] and Zhengming Sheng[1,2,4]
[1)] *Key Laboratory for Laser Plasmas (MOE), School of Physics and Astronomy, Shanghai Jiao Tong University, Shanghai, 200240, China*
[2)] *Collaborative Innovation Center of IFSA (CICIFSA), Shanghai Jiao Tong University, Shanghai 200240, China*
[3)] *Centre de Physique Théorique(CPHT), CNRS, Ecole Polytechnique, IP Paris, 91128 Palaiseau, France*
[4)] *Tsung-Dao Lee Institute, Shanghai Jiao Tong University, Shanghai 200240, China*

Previous studies have shown that the use of laser bandwidth may mitigate the growth of stimulated Raman scattering (SRS) in laser plasma interaction experiments, in particular when the spectrum of the driving (or pump) laser is composed of uniformly distributed frequency components with a well-chosen bandwidth [for example, M. Luo et al, Phys. Plasmas 29, 032102 (2022); H. Wen et al, Phys. Plasmas 28, 042109 (2021); R. K. Follett et al, Phys. Plasmas 26, 062111 (2019)]. Here, we investigate the effects of frequency chirp in the pump laser on backward SRS in inhomogeneous plasmas, taking into account kinetic effects associated with the nonlinear detuning of the parametric resonance due to high-amplitude electron plasma waves (EPW). Via theoretical considerations and numerical simulations, using a multi-dimensional particle-in-cell (PIC) code, it is shown that positive frequency chirp rates lead to a displacement of the resonance in the plasma profile. For a sufficiently strong positive chirp rate, such that the resonance displacement is faster than the EPW group velocity, the EPWs prove to remain limited in amplitude such that SRS is suppressed. The required frequency chirp rate corresponds to a laser bandwidth of about 1-2%.

I. INTRODUCTION

Stimulated Raman scattering (SRS) in plasmas is a parametric resonant three-wave interaction process, in which the laser light (the pump wave) scatters off an electron plasma wave (EPW), leading to a second electromagnetic wave (the scattered light wave). In the context of Inertial Confinement Fusion (ICF) with lasers, SRS may considerably reduce the coupling efficiency of the laser light to the plasma corona of the target through backscattering of the laser light and the generation of hot electrons. For this reason, it is essential to get a profound understanding of this SRS instability process and to find a way to get control over it. SRS occurs in coronal plasmas with electron densities n_e below the quarter-critical density (n_e<$n_{cr}/4$). Those plasmas are mostly inhomogeneous in ICF experiments. In typical experiments related to direct-drive ICF and shock ignition, SRS excitation has been reported mostly for plasma densities in the range from 4% to 10% n_{cr} with gradient scale lengths of several hundred laser wave lengths and at temperatures of a few keV[1,2]. In the presence of a density gradient, the amplification of the scattered light may be limited by the mismatch of the resonance condition. The spatial amplification over a spatially limited region in a linear profile can be described, following Rosenbluth's work[3], by exponential growth, $\sim \exp(G_R)$ with the gain coefficient G_R which depends on laser intensity and the gradient. However, increasing amplitudes of the driven EPWs may destabilize this type of solution due to the generation of trapped particles and thus lead to the inflationary regime of SRS[4–7]. In parabolic profiles with particular threshold conditions, SRS may be absolutely unstable.

Sufficiently large bandwidth, introducing temporal incoherence into the pump laser wave, may suppress the SRS instability. Previous theoretical studies[8,9] have shown that the frequency bandwidth, $\Delta\omega_0$, of the pump laser can effectively reduce the instability growth rate of SRS by a factor of $\gamma_0/\Delta\omega_0$, provided that $\gamma_0 < \Delta\omega_0$, where γ_0 denotes the SRS standard growth rate in a homogeneous plasma[10]. There are currently promising technological efforts to improve the efficiency of laser bandwidth in major laser facilities, like, e.g., the 'StarDriver' and 'spectral distribution' concepts[11,12]. Recently, simulations by use of the $LPSE$ code have proven that the multi-mode bandwidth can increase the threshold of absolute instability growth of SRS[13,14]. Zhao et al. have found that a decoupled broadband laser (DBL) with 10% bandwidth can completely suppress SRS[15]. Spatio-temporal optical smoothing techniques using spectral dispersion (SSD)[16–18] have been developed to introduce incoherence into laser beams, and can be combined with polarisation smoothing[19–21]. SSD, however, needs to be operated at large bandwidth to achieve a mitigating effect on SRS. Meanwhile, the idea of sunlight-like lasers with both random phase and polarization has been proposed[22] to suppress the SRS. In the work by H. Wen et al.[23], it is suggested that inflationary SRS can be mitigated by tuning the modulation frequency of the pump laser. On the other hand, although bandwidth generally reduces the growth rate, the interaction region around the exact resonance point in the plasma is broadened[24]. The EPW

[a)] Electronic mail: mufei.luo@polytechnique.edu

then stays inside the interaction region for a longer time interval before leaving. Consequently, the scattered light can still be amplified to a high level. This effect is more significant in multi-dimensional geometry, in particular for optically smoothed laser beams with speckles[25]. The EPW driven by intense speckles can be continuously amplified until leaving the speckles unless other nonlinear saturation mechanisms come into play, mostly due to kinetic effects[1,26–28]. Generally, the time the EPW wave trains stay inside a speckle, $\Delta t \sim \pi\lambda_0 F^2/v_L$, could be longer than the time for e-fold growth, $1/\gamma_0$, associated with the SRS instability growth rate γ_0, where λ_0 is the laser wavelength, v_L is the group velocity of the EPW, and F is the f-number of the laser.

Moreover, the previous studies on the mitigation of the SRS with broadband lasers usually assume that the different frequency components are distributed randomly or uniformly in the time domain within the laser duration. An interesting alternative to broadband lasers obtained via the random overlap of modes is the use of laser light fields modified by a chirp in the frequency. The frequency chirp has been found to be an important laser parameter for many applications in different areas, such as the technique of chirped pulse amplification (CPA)[29], optimizing/quenching the amplification and compression of short pulses by SRS[30–33], as well as in the strong-coupling regime of stimulated Brillouin scattering[34–36]. It is also possible to drive nonlinear ion-acoustic waves[37,38] and Bernstein-Greene-Kruskal (BGK) modes[39,40] through frequency chirp. The effect of chirped pulses in the context of SRS has been studied experimentally and theoretically with priority in the moderately relativistic regime[41–43], for which growth of forward and side scattering has still been seen at the back of the pulse.

In this work, we investigate the effect of frequency chirp on SRS, in particular its potential for mitigation on the SRS growth. It is shown that the resonant excitation of the EPW is governed by propagation in the presence of a chirp. This propagation velocity results from the cancellation between the chirp phase and the resonance mismatch due to the density gradient. Since it can be faster than the group velocity of the EPW for a particular chirp rate regime, the EPW can leave the interaction region quickly before being amplified to a noticeable level. Notably, in the presence of trapped-particle effects, which are responsible for the kinetic inflation observed in simulations[6,26–28] and experiments[44,45], the cancellation between the chirp phase and the resonance mismatch for the resonant EPW excitation is adjusted by the kinetic effects, or the nonlinear frequency downshift of the EPW. In this kinetic regime, the effects due to frequency chirp should therefore be significant, because they can result in both enhancement or reduction of SRS. Compared with previous work on SRS mitigation with broadband lasers, our theory and our results will show that a pump frequency chirp may be an effective alternative approach to control the structure of the excited EPW.

This paper is organized as follows. Section II presents the theory model of EPW excitation by the pump laser with frequency chirp. Based on this model, the spatio-temporal evolution of EPWs is studied in section III. The criterion for a critical frequency chirp value required to mitigate the EPW or SRS growth is derived, which is validated by numerical evaluation of the EPW equation. Particle-in-cell (PIC) simulation results are presented to validate our theory model in Sec. IV. The conclusions and discussions are given in Sec. V.

II. MODEL FOR THE PONDEROMOTIVELY DRIVEN PLASMA WAVE WITH LASER CHIRP

The evolution of the complex-valued amplitude f of the EPW, associated with the EPW's longitudinal electric field E_x in an underdense plasma can be written as[46]

$$\left[\frac{\partial}{\partial t} + v_L\frac{\partial}{\partial x} + i\sigma(x,x_r) + i\delta\omega_{\rm nl}\right] f = Pe^{i\psi}, \qquad (1)$$

wherein $P\exp(i\psi)$ is the driving term, σ stands for the frequency mismatch due to plasma inhomogeneity, v_L for the EPW's group velocity, and $\delta\omega_{\rm nl}$ for the nonlinear frequency shift, respectively. The temporal and spatial coordinates are normalized by $1/\omega_0$ and $1/k_0$, where ω_0 and k_0 are the laser frequency and wave number, respectively. The EPW amplitude f and the electric field E_x relate to each other as $eE_x/(m_e c\omega_{pe}) \equiv f\exp(-i\omega_L t + ik_L x) + c.c.$, with ω_L and k_L standing for the EPW's frequency and wave number, respectively, $\omega_{pe} = (n_e e^2/\epsilon_0 m_e)^{1/2}$ for the electron plasma frequency with the electron density n_e, the electron mass m_e and charge e, as well as the vacuum dielectric constant ϵ_0. As the driving term, we consider the ponderomotive force due to stimulated scattering via the coupling to the laser and the scattered electromagnetic fields, E_0 and E_1, respectively, with $P\exp(i\psi) \propto E_0 E_1$. In the frame of this model description, we consider a prescribed driver, and we take into account, via the phase ψ, the phase mismatch with respect to the resonance of stimulated scattering, as explained later on, induced by a laser chirp.

In Eq. (1), $\sigma(x,x_r)$ is the deviation from the resonance condition with respect to the resonance point x_r in an inhomogeneous plasma[3]. For a given linear plasma density profile $n_e = n_{e0}[1 + (x - x_r)/L]$ with L the gradient of the density profile, $\sigma(x,x_r) = v_L k' x$ by taking $x_r = 0$[4,5], with $k' = \omega^2_{pe(x=x_r)}/(6k_0^2 v_{th}^2 k_L L)$. Herein the EPW's group velocity v_L is normalized by the light velocity c in vacuum, $v_L \equiv 3v_{th}^2 k_L/(c\omega_L)$ with $v_{th} = (k_B T_e/m_e)^{1/2}$ being the thermal electron speed, k_B the Boltzmann constant, and T_e the electron temperature.

The nonlinear frequency shift $\delta\omega_{\rm nl}$ generally depends on the amplitude of the EPW. A key parameter to distinguish the nonlinear regimes of the EPW is the product between the EPW wave number k_L and the Debye length λ_D[47].

The regime with $k_L\lambda_D \lesssim 0.15$ is generally called the fluid regime, where the harmonics of the fundamental frequency ω_L of EPW lead to a frequency shift given by

$$\delta\omega_{\rm nl}(k_L\lambda_D \lesssim 0.15) = \zeta|f|^2, \tag{2}$$

to the lowest order. The factor ζ[48] describes the strength of the nonlinear fluid frequency shift, and it depends on plasma density and temperature[49–51].

In contrast to this, the regime with $k_L\lambda_D \gtrsim 0.25$, is called kinetic regime, in which the dominant nonlinearity comes from trapped particles, which can create a plateau in the electron velocity distribution function (VDF). This result in reduced nonlinear Landau damping and in a modification of the EPW dispersion relation, that can be expressed again via a frequency shift. This 'kinetic' frequency shift can be written as

$$\delta\omega_{\rm nl}(k_L\lambda_D \gtrsim 0.25) = -\eta\omega_L \left|\frac{\delta n_e}{n_0}\right|^{1/2} = -\beta|f|^{1/2}, \tag{3}$$

with $\beta = \eta\omega_L[(k_L/k_0)\sqrt{n_0/n_e}]^{1/2}$ and with $|\delta n_e/n_0|$ as the relative density perturbation. The amplitude-dependent frequency shift has been derived in the seminal work by Morales and O'Neil[52], with η as the kinetic factor depending on the second derivative of the electron distribution function evaluated at the phase velocity ω_L/k_L.

The two regimes, the so-called fluid regime and kinetic regime, can be distinguished from each other in the dynamics of the propagating EPW, due to the different power dependence of $\delta\omega_{\rm nl}$ on the EPW amplitude $|f|$, namely $|f|^2$ and $|f|^{1/2}$, respectively.

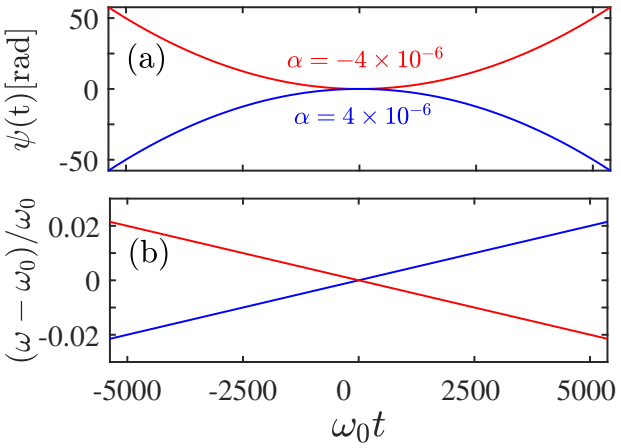

FIG. 1. (a) Behaviour of the phase of the chirped laser field as function of time and (b) the corresponding instantaneous departure of the laser frequency from its central frequency ω_0, here evaluated in $\omega_0 t = 1.88t/(fs\cdot\lambda_0/\mu m)$ for two different values of the chirp parameter $\alpha = \pm 4\times10^{-6}$ by setting $x = x_0$ and $t_0 = 0$.

For the phase of the prescribed drive, ψ, we consider here the phase of a chirped pump laser field, which can be approximated by[34,35]

$$\psi = -\frac{\alpha}{2}[(x-x_0)-(t-t_0)]^2, \tag{4}$$

where α is the chirp rate. One can define the instantaneous frequency and wave number of the pump laser as

$$\omega = 1-\partial_t\psi = 1-\alpha[(x-x_0)-(t-t_0)], \tag{5}$$
$$k = 1+\partial_x\psi = 1-\alpha[(x-x_0)-(t-t_0)]. \tag{6}$$

The instantaneous frequency depends on the position and is linear in time at a given position or linear in space at a given time. An example of the chirp phase and frequency via time $\omega_0 t = 1.88t/(fs\cdot\lambda_0/\mu m)$ is shown in Fig. 1, by setting $x = x_0$ and $t_0 = 0$.

III. ANALYSIS AND NUMERICAL SOLUTIONS

A. Threshold of frequency chirp for SRS mitigation

In recent work[6,53], the inflationary growth of SRS and hot electron generation in the kinetic regime has been studied with kinetic simulation codes. Also in experiments, the signatures of kinetic inflation have been observed[44,45]. We, therefore, concentrate in the following on the impact of a chirped pump laser pulse in the kinetic regime of SRS. As reference parameters, in consistency with plasma parameters for the kinetic regime in the experimental studies, we refer to an electron temperature of 1keV and an electron density of $n_{e0} = 0.05n_{cr}$ in the center of the inhomogeneous plasma profile, where n_{cr} is the critical density corresponding to a laser frequency ω_0. At the plasma center, these parameters yield hence $k_L\lambda_D = 0.34$, so that kinetic effects are expected to occur[47]. The model equation for the EPW reads in this regime

$$\left(\frac{\partial}{\partial t} + v_L\frac{\partial}{\partial x} + iv_L k' x - i\beta|f|^{1/2}\right) f = Pe^{i\psi}. \tag{7}$$

Replacing f by $\hat{f} = f\exp(-i\psi)$ with ψ defined in Eq. (4), and setting $x_0 = t_0 = 0$, Eq. (7) can be reduced to

$$\left(\frac{\partial}{\partial t} + v_L\frac{\partial}{\partial x} + i\delta\omega\right)\hat{f} = P, \tag{8}$$

where $\delta\omega = \alpha(x-t)(1-v_L) + v_L k' x - \beta|\hat{f}|^{1/2}$ is the total frequency shift of the EPW contributed by the frequency chirp, the resonance mismatch due to density inhomogeneity, and the nonlinear frequency shift due to the kinetic effect.

Following Chapman et al.[4] and Yaakobi et al.[54], we look for solutions that can be a guide line to describe the spatial-temporal evolution of the EPW amplitude. In analogy to Chapman and Yaakobi, that kind of solution is obtained by the mutual cancellation of several terms

of mismatch. Here we have resonance mismatch from the inhomogeneity, from the nonlinear kinetic frequency shift, and from the chirp phase. These three terms could dominate the EPW's evolution and adjust each other, resulting via $\delta\omega \equiv 0$ in the solution of $|\hat{f}|$ that reads

$$|\hat{f}| = \left[\frac{\alpha(x-t)(1-v_L) + v_L k' x}{\beta}\right]^2. \quad (9)$$

This behavior of $|\hat{f}|$ neglects the influence of the right-hand side of the equation involving the ponderomotive drive along the characteristics $s = x - v_L t$ running at a slower speed than the light velocity, namely $v_L < 1$.

Before proceeding to numerical integration of Eq. (7), we assume for the following discussion that the nonlinear evolution of $\hat{f}$ is dominated by the solution Eq. (9). Note that Eq. (9) reduces to the solution discussed in Ref. 4 by neglecting the frequency chirp, i.e. $\alpha = 0$. The involvement of the frequency chirp introduces the time-dependence via a displacement to the shape of the solution governed by Eq. (9), while the shape of the solution in Ref. 4 is stationary. The displacement of the parabolic shape in space obtained from the solution Eq. (9) can be obtained by setting $|\hat{f}| = \text{const}$ and, subsequently, by differentiating in time, which yields $\alpha(dx/dt - 1)(1 - v_L) + v_L k' dx/dt = 0$, and the 'resonant velocity' we can call is given by

$$v_{re} = \frac{dx}{dt} = \frac{\alpha(1-v_L)}{\alpha(1-v_L) + v_L k'}, \quad (10)$$

which describes the propagation of the resonant excitation of the EPW. From this expression, it results that in a plasma with a positive gradient density, v_{re} can be negative for negative chirp $\alpha < 0$, while it is positive for positive $\alpha > 0$. It is important to note that v_{re} can exceed the group velocity v_L for $\alpha > v_L^2 k'/(1-v_L)^2$. Under the condition for a strong enough chirp with $\alpha > v_L^2 k'/(1-v_L)^2$, the EPW is hence able to leave the interaction region quickly before being further amplified to a noticeable level. Consequently, via an adequate choice of α, the chirp can be used to mitigate the growth of EPW. For this reason, we define α_c as the critical chirp rate,

$$\alpha_c = v_L^2 k'/(1-v_L)^2. \quad (11)$$

We will see in the following that expression Eq. (11) indicates indeed the threshold of frequency chirp for SRS mitigation in a positive gradient density plasma. Under the given plasma and laser parameters, the resonant velocity v_{re}, as a function of α, is shown in Fig. 2. The gradient of the density profile here is $k_0 L = 1790$. The horizontal red and blue lines are the particular cases with $\alpha = 0$ and $\alpha = \alpha_c$, resulting in $v_{re} = 0$ and $v_{re} = v_L$, respectively.

It should be noted that Eq. (9) has been obtained by setting $x_0 = t_0 = 0$, for simplicity. In particular, the choice of a non-zero value of t_0 means that the interaction

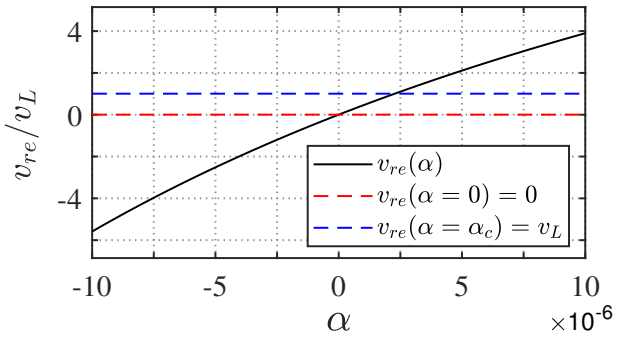

FIG. 2. Resonant velocity v_{re} defined by Eq. (10) in the unit of the group velocity v_L of EPW, as function of the chirp rate α. The horizontal red and blue lines are the particular cases when $\alpha = 0$ and $\alpha = \alpha_c$, resulting in $v_{re} = 0$ and $v_{re} = v_L$, respectively.

to excite the EPW is not synchronized with the onset of the chirp, such that it starts with a chirp phase of $\psi = -\alpha t_0^2/2$, or an initial frequency shift $-\alpha t_0$ to the central laser frequency ω_0. See Appendix for a further discussion of a non-zero value of t_0 effect on the EPW excitation.

B. Dependence of EPW saturation amplitude on frequency chirp

By setting $x_0 = t_0 = 0$, we numerically solve Eq. (7) with a constant amplitude $P = 2.1 \times 10^{-6}$ and with the kinetic factor η=0.25, such that β =0.18. For this choice of η, we refer to Refs. 5 and 55. The evolution of the EPW in the form of $|\delta n_e/n_0|$ is shown in Fig. 3, where $|\delta n_e/n_0| = (k_L/\omega_{pe})|f|$. The color lines in Figs. 3(a)(c)(e) and (g) represent the spatial profiles of the envelope of the EPW at a series of 4 time instants, from $\omega_0 t$ =2683 to 10733, while Figs. 3(b)(d)(f) and (h) show its spatio-temporal evolution. As one can see, the different chirp values, from negative $\alpha = -10^{-6}$ to positive $+4 \times 10^{-6}$, alter considerably the evolution of the EPW envelope. In the subplots (a) and (b) of Fig. 3, where the chirp rate is negative with $\alpha = -10^{-6}$, also the resonant velocity v_{re} is negative. The rear edge of the EPW envelope closely follows the curve governed by Eq. (9) (indicated by the black dashed line), and it propagates in the backward direction with velocity v_{re} (indicated by the black solid arrow in Fig. 3(b)); still, the front edge propagates in the forward direction with the group velocity v_L of the EPW as indicated by the black dashed arrow in Fig. 3(b). In Figs. 3(c) and (d) when no chirp is applied, one encounters the situation as obtained in the study by Chapman et al.[4]. By increasing the chirp rate to positive values, as shown in Figs. 3(e) and (f) where $\alpha = 10^{-6}$, the resonant velocity v_{re} becomes positive, while it is still smaller than the group velocity v_L. The rear edge of the EPW is still well described by Eq.

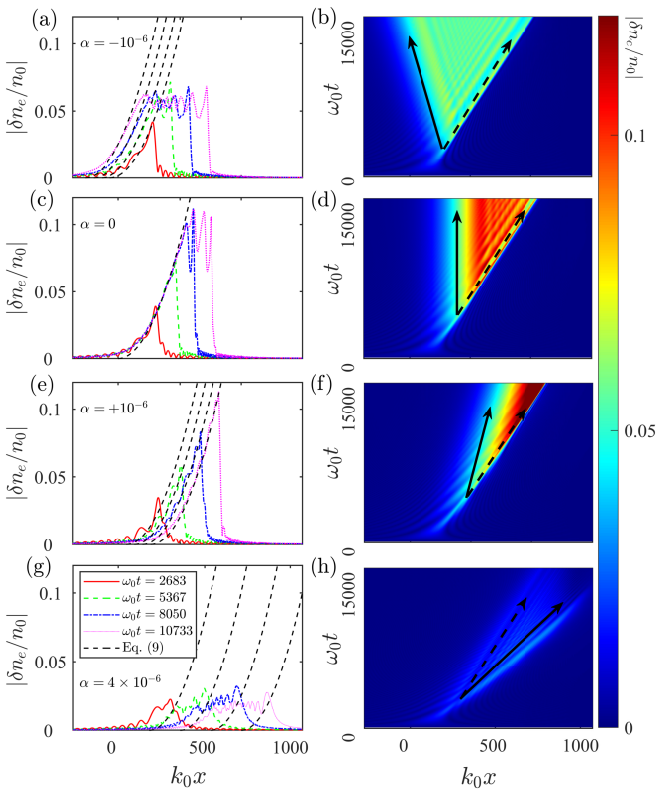

FIG. 3. Numerical solutions to the prescribed EPW Eq. (7), showing the growth and propagation of EPW in plasma with a positive density gradient. The spatial growth of the EPW at different instants with different chirp rates are shown in (a) $\alpha = -10^{-6}$, (c) $\alpha = 0$, (e) $\alpha = 10^{-6}$ and (g) $\alpha = 4 \times 10^{-6}$. The black dashed lines mark the curve Eq. (9); (b)(d)(f) and (h) show the spatial-temporal evolution of EPW with the corresponding chirp rates in (a)(c)(e) and (g), where the black solid arrow represents v_{re} defined via Eq. (10), and the black dashed arrow represents the group velocity v_L of EPW.

(9), and it propagates at velocity v_{re}, which is slower than the front edge, propagating at group velocity v_L. Note that for this case, the maximum EPW amplitude attained is still high, as for the case without a chirp, of the order of 0.1. Now, increasing the chirp rate to a value above the critical chirp value, namely $\alpha_c = 2.3 \times 10^{-6}$, as illustrated in Figs. 3(g) and (h) where $\alpha = 4 \times 10^{-6}$, the resonant velocity v_{re} then is higher than the group velocity v_L. In this case, the front edge of the EPW propagates at the resonant velocity v_{re}, while, now, the rear edge propagates at group velocity v_L. This has the consequence that the EPW can no longer follow the solution associated with Eq. (9), which is clearly observable in inspecting the no longer parabolic shape of the EPW rear edge and the much smaller amplitudes attained with respect to the cases with a smaller chirp. The four cases mentioned above show that the choice of an adequate frequency chirp yields the potential to detune the resonance or break the phase-locking during the interaction, which provides a new route to suppress SRS.

It is worth noting that the formalism of Eq. (10) is independent of the kinetic factor η or β. Indeed by setting $\eta = 0$, we have seen a similar feature, i.e., the excitation of EPW happens inside the domain, whose one boundary propagates with v_L and another one propagates with v_{re}. This results naturally from the cancellation between the detuning brought by frequency chirp and the resonance mismatch due to density inhomogeneity. The participation of the nonlinear frequency shift could adjust this cancellation, and the adjustment makes the EPW profile be well predicted by Eq. (9).

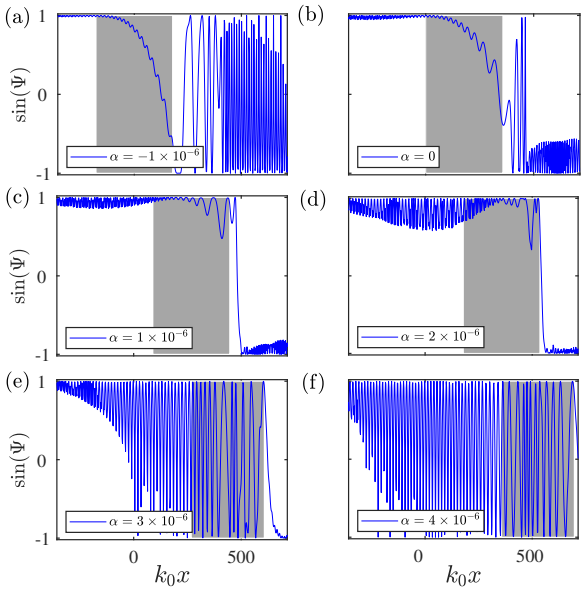

FIG. 4. Numerical solutions of the prescribed EPW Eq. (7), showing the spatial variation of the phase Ψ in the complex envelope of EPW at one instant, where $\Psi = \mathrm{Arg}(f) - \psi$. The chirp rates α in (a)(b)(c) and (d) are smaller than α_c. An apparent phase-locking region is shown, where phase Ψ is locked at around $\pi/2$. The shadows mark the growing region of EPW. In (e) and (f) with α larger than α_c, no obvious phase-locking region is observed inside the shadow.

To further understand the physics of the EPW excitation governed by the frequency chirp, the mismatch from resonance, and the frequency shift due to nonlinear kinetic EPW, we extract the phase $\mathrm{Arg}(f)$ from the complex amplitude of the EPW, and calculate its difference to the chirp phase ψ, namely, $\Psi = \mathrm{Arg}(f) - \psi$. The snapshots of $\sin(\Psi)$-value of the phase Ψ at one time instant, but for different chirp rates, are shown in Fig. 4 (blue solid lines). The shadows mark the areas where EPWs are driven. The chirp rate α ranges from -10^{-6} to 4×10^{-6}, and the resonant velocity v_{re} varies from negative to positive values, up to the range when the resonance point moves faster than the group velocity, i.e., $v_{re} > v_L$. For the choice of chirp rates $\alpha < \alpha_c$ in Figs. 4(a-d), the corresponding velocity v_{re} is slower than the group velocity v_L. The quantity Ψ is locked around $\pi/2$, yielding $\sin(\Psi) \approx 1$ within the shadow. This phase-locking promotes the growth of the EPW. While

in Figs. 4(e) and (f), the chirp rate α exceeds α_c, leading to $v_{re} > v_L$, for which a stable phase-locking area cannot be established. The breaking of phase locking suppresses the growth of the EPW, as one sees in Fig. 3(g) or (h).

The spatio-temporal evolution of $\sin(\Psi)$ is shown in Fig. 5 for the two cases with $\alpha = 2 \times 10^{-6}$ in (a) and 3×10^{-6} in (b). These two values of α are respectively located at two sides of the critical value α_c. Obviously, a stable phase-locking area is established in Fig. 5(a), where the black ellipse marks the region in which the EPW is excited. On the contrary, the phase-locking is destroyed for the larger positive chirp rate in Fig. 5(b). Both Fig. 4 and Fig. 5 suggest that the choice of the chirp rate can determine whether an apparent phase-locking exists or not, and this can lead to enhancement or mitigation of the SRS.

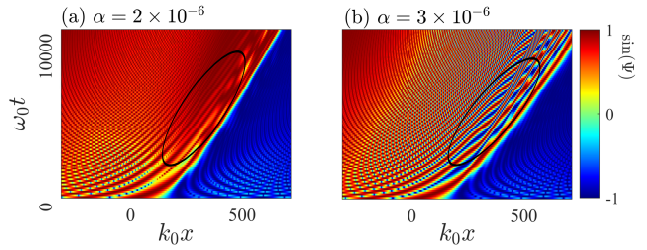

FIG. 5. Spatio-temporal evolution of the phase Ψ for different chirp rates, where $\Psi = \mathrm{Arg}(f) - \psi$. The black ellipses indicate the area where the EPW is excited. The critical value α_c is located between $\alpha = 2 \times 10^{-6}$ (a) to $\alpha = 3 \times 10^{-6}$ (b).

Considering the existence of the phase-locking for $\alpha < \alpha_c$, it allows us to develop a model to estimate the limit of the EPW amplitude, as it is driven when the phase-locking can be maintained. Our model is based upon the variational approach, which is analogous to that in Refs. 4, 56, and 57. By substituting $\hat{f} = |\hat{f}|e^{i\Psi}$ into Eq. (8), one obtains

$$\frac{\partial_t J}{v_L} + \partial_x J = \frac{2P}{v_L} J^{1/2} \cos(\Psi), \tag{12}$$

$$\frac{\partial_t \Psi}{v_L} + \partial_x \Psi = -\frac{P}{v_L J^{1/2}} \sin(\Psi) - \delta\omega/v_L, \tag{13}$$

where $J = |\hat{f}|^2$ is the action of the system. Within the phase-locking area, the phase is locked at $\Psi \approx \pi/2$, and the action J can be divided into a slowly varying average action $\bar{J}$ and a perturbation Σ, such that $J = \bar{J} + \Sigma$. Following the variational process similar to Ref. 4, a Hamiltonian system $H = H(x, \Psi, \Sigma)$ can be established,

$$H = \frac{1}{2\mathcal{M}}(\mathcal{M}\Sigma)^2 + V_l + V_o, \tag{14}$$

which describes a pseudo-particle with the effective pseudo-mass $\mathcal{M}$ moving in a pseudo-potential. The pseudo-potential can be divided into the linear part V_l and the oscillatory part V_o, given by

$$V_l = \Psi \frac{[\alpha(1-v_L) + v_L k'']/v_L - [\alpha(1-v_L)]/v_L^2}{\mathcal{M}}, \tag{15}$$

$$V_o = -\frac{2P}{v_L} \bar{J}^{1/2} \sin(\Psi), \tag{16}$$

and $\mathcal{M} = \beta/(4v_L\bar{J}^{3/4}) + P/(2v_L\bar{J}^{3/2})$. Clearly, if the pseudo-particle remains trapped inside the pseudo-potential, keeping a small oscillation around a locked value of Ψ, the force coming from V_o should be strong enough as compared to the force coming from V_l, resulting in a local minimum in the pseudo-potential. Then the condition is given by

$$\left|\frac{dV_o}{d\Psi}\right|_{max} > \left|\frac{dV_l}{d\Psi}\right|, \tag{17}$$

which yields

$$\bar{J}^{1/4} < \frac{P\beta}{2[\alpha(1-v_L) + v_L k''](v_L - v_{re})}. \tag{18}$$

Here we take $\mathcal{M} \approx \beta/(4v_L\bar{J}^{3/4})$, which is a good approximation for the parameters given earlier. In absence of chirp, inequality (18) returns back to the one mentioned in Ref. 4. In the particular case, when increasing α to approach α_c, i.e., v_{re} approaching v_L, the right-hand-side of inequality (18) diverges, indicating that there is no limitation on the EPW's growth. Moreover, when α exceeds α_c, i.e., v_{re} exceeding v_L, the right-hand-side term of (18) becomes negative. Both situations make no physical sense. These non-physical situations exactly invalidate the assumption of phase-locking. Namely, this illustrates that the frequency chirp can destroy the phase-locking provided the chirp rate α approaches or exceeds α_c. In this case, the resonant velocity v_{re} becomes faster than the group velocity v_L, and under which the mitigation of the EPW amplitude is expected. This is what we see in Figs. 3(g)(h) and Figs. 4(e)(f).

In Fig. 6 we have plotted the squares of the right-hand-side values of inequality (18) as a function of α for $\alpha < \alpha_c$. In the same plot, we also show the numerically determined maximum EPW amplitude $|\delta n_e/n_0|_m$, either with or without kinetic effects included. Typically, the maximum amplitude $|\delta n_e/n_0|_m$ in the absence of kinetic effects shown by the blue diamond line is smaller, where the dominant detuning mechanisms are density inhomogeneity and frequency chirp. Only when these two terms cancel each other, a peak value appears. Namely, $v_L k'' x$ cancels $\alpha(x-t)(1-v_L)$ by replacing t by x/v_{re}, and v_{re} equals to v_L with $\alpha = \alpha_c$.

However, by taking into account the kinetic frequency shift, the value of $|\delta n_e/n_0|_m$ shown by the red circular line is higher than that in the former case with $\alpha < \alpha_c$. This is due to the broadened phase-locking area discussed above, which promotes the growth of the EPW. Meanwhile, the tendency of this part in the red circular line is well described by the black dashed line, the upper limit of inequality (18). For $\alpha > \alpha_c$, the frequency chirp is

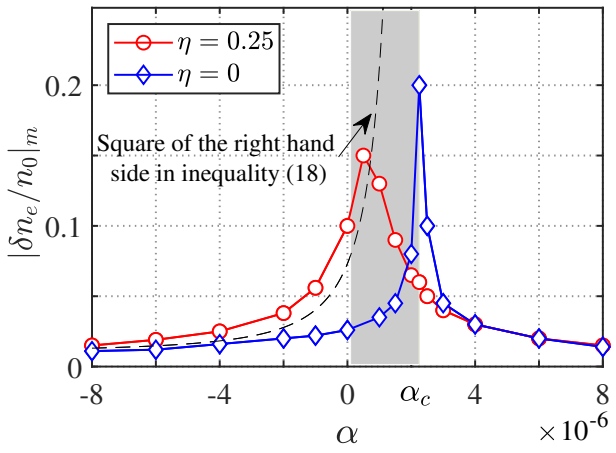

FIG. 6. The maximum $|\delta n_e/n_0|_m$ found from the numerical computation is shown as a function of the chirp rate α either with or without considering the kinetic frequency shift by setting $\eta = 0.25$ or $\eta = 0$. The black dashed line is the upper limit in inequality (18) for $\alpha < \alpha_c$.

able to break the phase-locking. Subsequently, the value of $|\delta n_e/n_0|_m$ returns to that shown by the blue line. In addition, the interval $\alpha \in (0, \alpha_c]$ marked by the shadow is regarded as the transition region.

IV. PARTICLE-IN-CELL SIMULATIONS

A. Simulation setup

Kinetic simulations, by using the one (1D) and two-dimensional (2D) version of the electromagnetic PIC code EPOCH[58], have been performed to investigate the effects of frequency chirp in SRS. All the simulations presented here have been carried out in the same geometry. The plasma parameters are the same as that mentioned in Sec. III, with the plasma density profile $n_e = 0.05 n_{cr}(1 + x/1790)$, and with the electron temperature $T_e = 1$keV. Ions are set to be fixed as a neutral background. In the 1D case, the simulation window has a length of $k_0 L_x = 2864$, and a $k_0 L_p = 2685$ plasma slab is chosen with approximately $k_0 L_v = 90$ vacuum space on either side of the plasma region. In the 2D case, to limit the computational expense, the longitudinal and transverse sizes of the simulation window are $k_0 L_x = 1970$ and $k_0 L_y = 215$, respectively, with a $k_0 L_p = 1790$ plasma slab. The laser used in the 2D case is a Gaussian beam injected from the left side with $F = 5$, the f-number of the laser, and focused at $k_0 x = -180$ in the longitudinal direction and at the middle of the transverse direction. This 2D configuration is motivated by finding a path to decrease the coupling between the incident pump laser and EPW through frequency chirp, thereby mitigating the SRS.

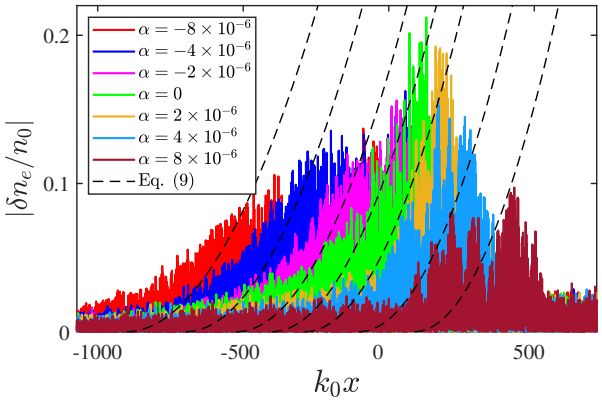

FIG. 7. Snapshots of the EPW amplitude, taken at time $\omega_0 t = 4830$, for different chirp rates obtained from 1D PIC simulation. The EPW is driven by two counter-propagating electromagnetic fields (pump and seed) in a plasma profile with a positive density gradient. The black dashed lines represent the curve of Eq. (9).

B. 1D PIC simulation results

Firstly, to validate the above theory and Eq. (9) and Eq. (10), a single-mode of EPW is driven by two counter-propagating electromagnetic fields. The incident pump laser field is injected from the left side with an intensity of $I_0 \lambda_0^2 = 6.16 \times 10^{14}\mathrm{W/cm^2}\mu\mathrm{m}^2$, while the seed light is injected from the right side with $I_1 \lambda_1^2 = 2.24 \times 10^{12}\mathrm{W/cm^2}\mu\mathrm{m}^2$. The choice of wavelengths should satisfy the matching condition at one reference point. Here this reference point is taken at $k_0 x = 0$ with density $n_{e0} = 0.05 n_{cr}$.

The EPW amplitudes corresponding to the different choices of the chirp rate α at one time instant are shown in Fig. 7, accompanied by the curves that correspond to Eq. (9). The density perturbation $|\delta n_e/n_0|$ have been deduced from the longitudinal electrical field E_x via Poisson's equation $|\delta n_e/n_0| = |E_x|\epsilon_0 k_L/(n_e e)$. The comparison illustrates that the key features showing the influence of the frequency chirp on the EPW evolution, indicated in Sec. III, are reproduced. As stated above, the three detuning mechanisms including the frequency chirp, the resonance mismatch from density inhomogeneity, and the non-negligible kinetic effects together lead to the evolution of EPW, which is described by Eq. (9). Specifically, the rear or front edge of the EPW with the choice of the chirp value $\alpha < \alpha_c$ or $\alpha > \alpha_c$ closely follows the parabola curve of Eq. (9). Noting that the critical value α_c defined by Eq. (11) equals to 2.3×10^{-6} under the given parameters. One can also see that the maximum EPW amplitude as a function of α displays a similar tendency to the red line in Fig. 6.

The spatio-temporal evolution of the EPW is shown in Fig. 8. To highlight the effect of frequency chirp, relatively large chirp rates have been selected with $\alpha = \pm 8 \times 10^{-6}$. These choices can lead to quite large reso-

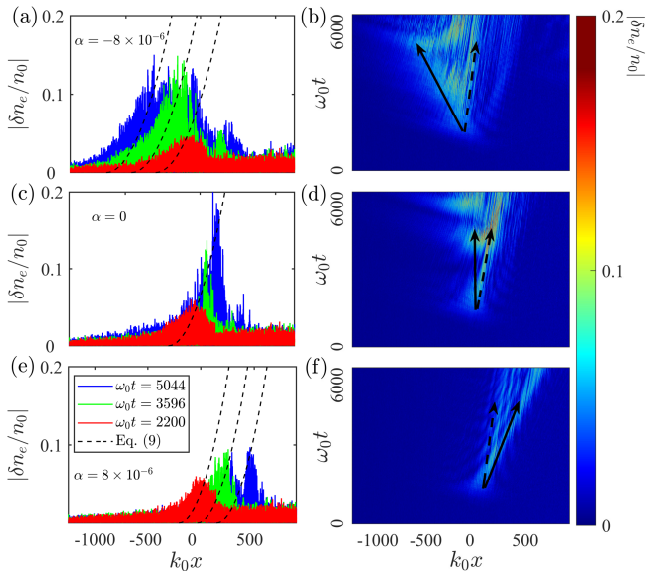

FIG. 8. PIC simulation results of the evolution of the EPW amplitude for different values of the frequency chirp. (a), (c), and (e) show the spatial growth of EPW at a series of instants with the corresponding chirp rates $\alpha = -8\times10^{-6}$ (a), $\alpha = 0$ (c), and $\alpha = 8\times10^{-6}$ (e). The black dashed lines mark the curve of Eq. (9); (b), (d), and (f) show the spatio-temporal evolution of EPW with the corresponding chirp rates in (a), (c), and (e), the black solid arrow represents resonant velocity v_{re} defined via Eq. (10), and the black dashed arrow represents the group velocity v_L of EPW.

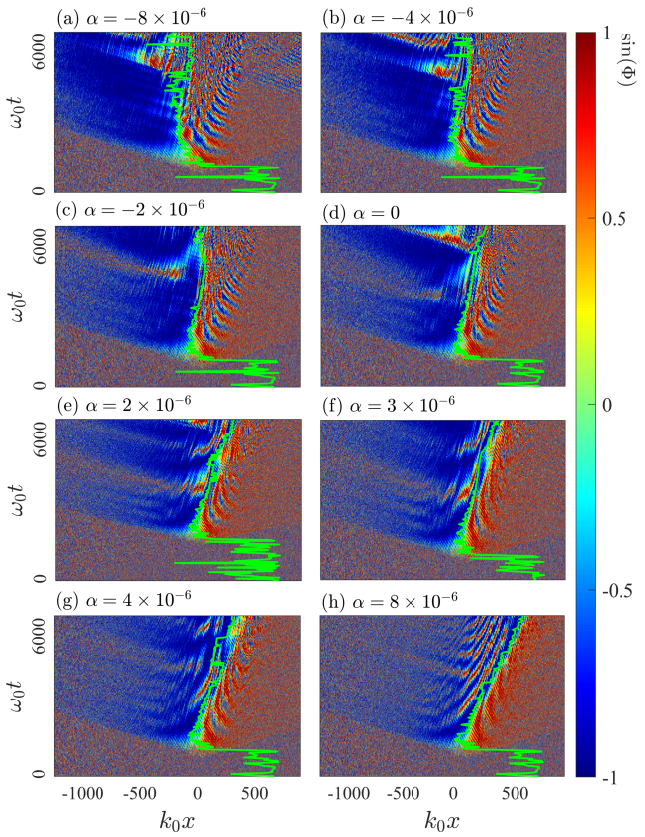

FIG. 9. Spatio-temporal evolution of $\sin(\Phi)$ for different frequency chirp rates, with the phase defined as $\Phi = \varphi_0 - \varphi_1 - \varphi_L$, and $\varphi_{0,1} = \mathrm{Arg}(E_{0,1})$, $E_{0,1}$ from the complex-valued envelopes of pump laser and scattered light. The chirp phase ψ is already introduced into φ_0, and $\varphi_L = \mathrm{Arg}(f)$ is the phase of the complex phase of EPW. The dark blue region with $\sin(\Phi) = -1$ is the phase-locking area. The green solid line represents the trajectory of spatial maximum EPW amplitude.

nant velocities v_{re}, such that the front or rear parts of the EPW can propagate over a long distance within a short time window. The EPW amplitudes taken from PIC simulations in a series of moments are shown in Figs. 8(a), (c), and (e), and their spatio-temporal evolution is shown in Figs. 8(b), (d), and (f), with $\alpha = -8\times10^{-6}$ in (a) and (b), $\alpha = 0$ in (c) and (d), and $\alpha = 8\times10^{-6}$ in (e) and (f). In Figs. 8(a), (c), and (e), the black dashed line is the curve of Eq. (9), and in Figs. 8(b), (d), and (f), the black dashed and solid arrows represent the group velocity v_L and the resonant velocity v_{re} calculated from Eq. (10), respectively. Again for $\alpha < \alpha_c$ in Figs. 8(a) and (b), the rear part of the EPW amplitude is well described by Eq. (9), and propagates backward at velocity v_{re}. In contrast to the latter, for $\alpha > \alpha_c$ in Figs. 8(e) and (f), the front part of the EPW amplitude follows only roughly the curve of Eq. (9), propagating at velocity v_{re}.

Analogous to Sec. III, the phase-locking area extracted from the PIC simulation is shown in Fig. 9. The phases have been extracted from PIC simulations via the method explained in Ref. 5, using Fourier transforms in k_x-space. It deserves attention that in Fig. 4, where a constant ponderomotive force is applied, the locking-phase shown there is $\Psi = \mathrm{Arg}\ (\hat{f}) = \mathrm{Arg}(f) - \psi$, with $\mathrm{Arg}(f)$ being the phase carried by the complex envelope of EPW and ψ the chirp phase. In the PIC simulation, however, the ponderomotive force from the beating between the pump laser and the scattered light is not a constant, hence the concerned locking-phase should be $\Phi = \varphi_0 - \varphi_1 - \varphi_L$, where $\varphi_{0,1} = \mathrm{Arg}(E_{0,1})$ with $E_{0,1}$ the complex-valued envelopes of the pump laser and scattered light, φ_0 already contains the chirp phase ψ. Here, $\varphi_L = \mathrm{Arg}(f)$ is still the phase of the complex-valued envelope of plasma waves[36,59,60]. Figure 9 shows the spatio-temporal behaviour of $\sin(\Phi)$, where the dark blue area with $\sin(\Phi) = -1$ indicates the phase-locking, and the green line is the trajectory of the spatial maximum EPW amplitude.

For Fig. 9(a) to (d), where the frequency chirp values are non-positive, the broad phase-locking area is established and mainly located at the left side. This is consistent with the direction of the resonant velocity v_{re}, which points in the opposite direction to the group velocity v_L. This phase-locking area becomes narrower as the chirp rate α increases according to Fig. 9(a) to (d). The tendency to a more limited area is related to the decreasing absolute value of v_{re}. This guarantees that the backward-

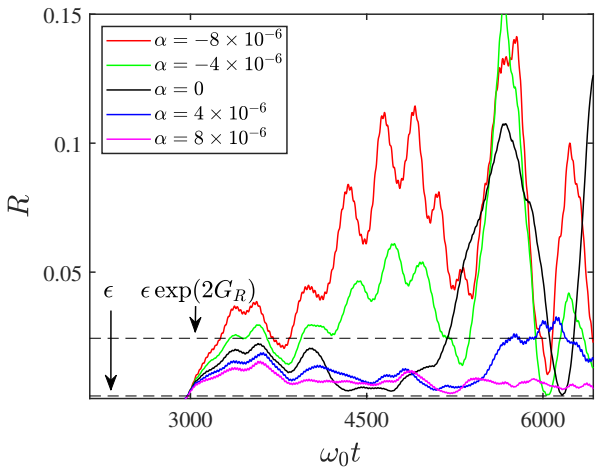

FIG. 10. Reflectivity from PIC simulations under different chirp rates. where the EPW is driven by two counter-propagating fields, the pump laser and the seed light fields in a plasma profile with a positive density gradient. Black dashed lines show the initial injected seed level and the scattered level expected after Rosenbluth amplification, in the unit of pump intensity.

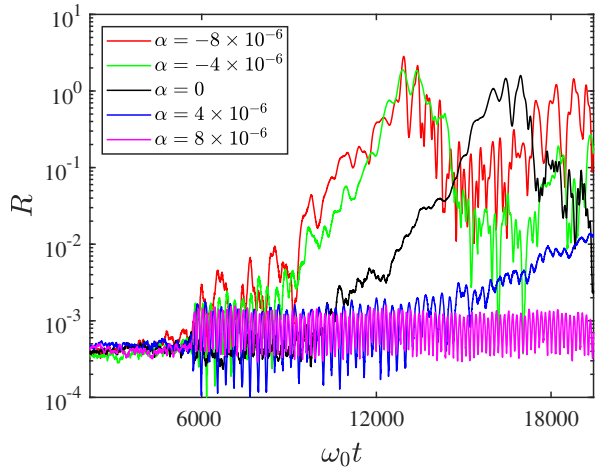

FIG. 11. Reflectivity from PIC simulations under different chirp rates, where EPW, in contrast to the case shown in Fig. 10, is seeded via the PIC background noise (i.e., $I_1 = 0$), together with the pump laser field. The noise level in PIC simulations exceeds the natural broadband noise level in plasmas.

propagating rear part of EPW could experience a clean background with phase-locking $\sin(\Phi) = -1$ to maintain its growth until the limit of the locking condition is met, referring to inequality (18). When increasing the chirp rate further to be positive as in Fig. 9(e) to (h), the chirp rate α will cross the critical value of α_c for Fig. 9(e) to (f). This leads to the change of v_{re} from being slower than v_L to faster than v_L. Obviously, within the right-side area where the EPW is driven, vibrations in the value of $\sin(\Phi)$ arise. The larger the value of α, the stronger are the arising vibrations as seen from Fig. 9(e) to (h). As discussed in Sec. III, and illustrated in Figs. 8(e), (f) and Fig. 9(h), this broken phase-locking helps to suppress the growth of EPW. Subsequently, this phase-locking behavior not only directly impacts the growth of EPW but also indirectly influences the SRS reflectivity.

The reflectivity defined as $R = I_{lhs}/I_0$ is shown in Fig. 10 by the colored lines, where I_{lhs} denotes the scattered light intensity taken from the left boundary. The EPW is driven by two counter-propagating electromagnetic fields, the pump laser and the seed light field, in the present case. The two dashed lines show the initial seed intensity $\epsilon = I_1/I_0$ in the unit of pump intensity and the scattering level predicted by Rosenbluth's theory[3] in the absence of any nonlinear effects, $\epsilon \exp(2G_R)$. The temporal evolution of R is shown within $\omega_0 t$=6440 to ensure the central part of the single-mode EPW does not reach the boundary. In the absence of chirp, the black curve exhibits the inflationary growth of the scattered light so that the reflectivity R exceeds Rosenbluth's prediction. This inflationary growth is accompanied by the locking phase shown in Fig. 9(d), as explained by the autoresonance mechanism[4,5]. While introducing the frequency chirp into the pump laser with negative chirp rates, where the red and green curves respectively show the results with $\alpha = -8 \times 10^{-6}$ and -4×10^{-6}, inflationary growth of the reflectivity occurs earlier than the case without frequency chirp. This is because the choice of a negative chirp rate leads to a broader phase-locking area, shown in Figs. 9(a) and 9(b), which promotes the scattering. In contrast to the choice of a negative chirp, the blue and pink curves are for cases with positive chirp rates, which show already mitigated scattering levels due to the destroyed phase-locking as displayed in Figs. 9(g) and (h).

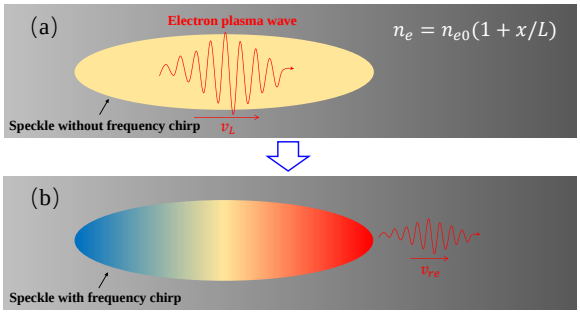

FIG. 12. Schematic presentation of EPW excitation in a 2D configuration with a laser speckle. (a) Without frequency chirp in the pump laser, the EPW propagates with group velocity v_L, where the coupling between the pump laser and EPW can be strong as the EPW can stay inside the speckle for a long time. (b) With a frequency chirp larger than α_c, the EPW can be dragged out of the excitation region quickly before it grows to a high level, thus the coupling between the pump laser and EPW could be reduced.

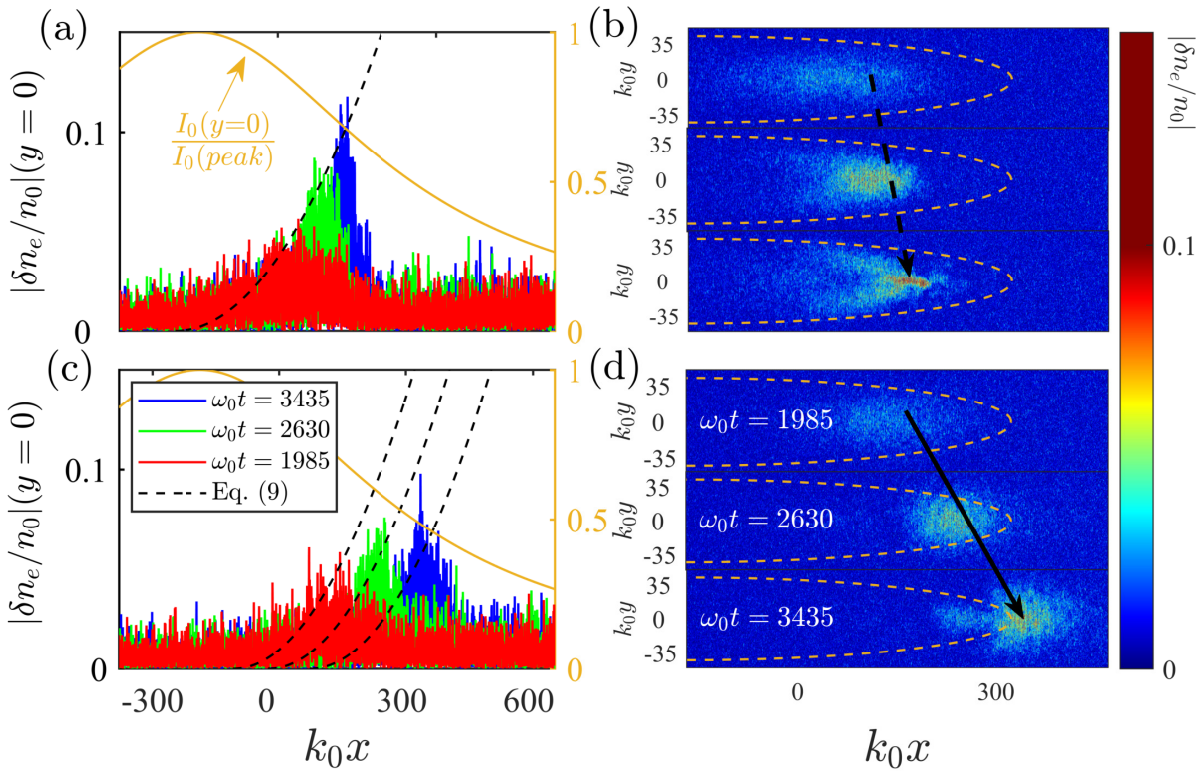

FIG. 13. 2D PIC simulation results of the EPW driven by the beating between a Gaussian pump laser and a counter-propagating plane seed wave. (a) and (b) show respectively the longitudinal spatial growth of EPW at transverse location $y = 0$ and the spatial-temporal evolution of EPW at a series of instants in the absence of the frequency chirp in the pump. The black dashed arrow in (b) marks the group velocity v_L. (c) and (d) show the case with frequency chirp in the pump with $\alpha = 8 \times 10^{-6}$, the black solid arrow in (d) marks the resonant velocity v_{re} defined via Eq. (10). The yellow solid lines in (a) and (c) are the longitudinal intensity profiles of the pump at transverse location $y = 0$ in the unit of its peak intensity. And the black dashed lines are from Eq. (9). The envelopes of the laser speckles are represented by the yellow ellipses in (b) and (d).

In the preceding case, the EPW carrying a single frequency is excited by two counter-propagating light fields with $I_1 \neq 0$. We now consider the growth of the SRS reflectivity for the more realistic case where the backscattered light is seeded by the background noise in the plasma, which exists naturally due to the electron density fluctuations. For this case, we consider letting $I_1 = 0$. A similar behavior of the reflectivity R is found in Fig. 11. The negative choice of chirp rates leads to more significant inflationary growth than that in the absence of chirp, while it shows a severely mitigated level by taking positive chirp rates.

C. 2D PIC simulation results

In Sec. IV B, the impact of frequency chirp on EPW excitation, phase-locking phenomenon, and the reflectivity from SRS were discussed in the 1D configuration, where the pump laser intensity remains constant along the longitudinal direction unless the pump depletion is significant. Although the resonant velocity v_{re}, at which the central growing part of EPW propagates, may be faster than the group velocity v_L of the EPW, and the phase-locking is damaged provided the chirp rate $\alpha > \alpha_c$, the EPW still feels the strong pump laser intensity in the 1D case.

Considering spatially smoothed lasers[25], in which a laser beam consists of numerous hot spots or speckles, EPWs are driven initially inside those hot spots, whose intensity is locally at a high level[61,62]. An intense speckle has a longitudinal size $k_0 l_\parallel \sim 2\pi^2 F^2$ and a transverse size $k_0 l_\perp \sim 2\pi F$. The EPW driven inside the speckle propagates at the group velocity v_L in the absence of chirp, as indicated in Fig. 12(a). When the longitudinal size of the speckle is relatively long, corresponding to a big f-number, the EPW could be amplified over a long distance and the onset of kinetic inflation for SRS can be expected. However, if frequency chirp is introduced into the laser with $\alpha > \alpha_c$, the excited EPW would move out of the intense speckle more quickly, and meanwhile the phase-locking is destroyed. Hence the reduction of the coupling between the EPW and the pump laser is expected as indicated in Fig. 12(b).

To illustrate this scenario in our 2D simulations, the peak intensity of the Gaussian laser beam is chosen

to be $I_0(peak)\lambda_0^2 = 8.62 \times 10^{14}\mathrm{W/cm^2}\mu\mathrm{m}^2$, and a counter-propagating wave as the seed light is injected from the right side with the intensity $I_1\lambda_1^2 = 1.57 \times 10^{12}\mathrm{W/cm^2}\mu\mathrm{m}^2$. This seed light has a Gaussian intensity profile $\sim \exp(-(y/w)^2)$ in the transverse direction, where $k_0 w = 35 \approx 2\pi F$. Still, the wavelengths of the pump and seed are chosen to allow the matching condition to be satisfied at the plasma center.

Significant spatial growth of EPW in the 2D configuration is seen in Fig. 13. Autoresonance behavior is exhibited in Fig. 13(a) in the absence of chirp, where snapshots of the EPW amplitude are at three instants at the transverse position with $k_0 y = 0$, the transverse center of the intense speckle. The growth of the EPW closely follows the curves governed by Eq. (9). The yellow solid line represents the laser intensity profile $I_0(x, y = 0)$ along the longitudinal direction in the unit of its peak value $I_0(peak)$. Within the time window of our simulation, the EPW propagates at group velocity v_L (the black dashed arrow) and stays inside the speckle as shown in Fig. 13(b), thus robust amplification of the EPW is expected due to the local intense spot. The envelope of the speckle is marked by the ellipses. In the presence of chirp with $\alpha = 8 \times 10^{-6} > \alpha_c$, Figs. 13(c)(d) show that the EPW exhibits a faster propagation speed at the resonant velocity v_{re}, which moves out of the speckle at $\omega_0 t = 3435$, as shown in Fig. 13(d), where the black solid arrow represents the velocity v_{re} defined by Eq. (10).

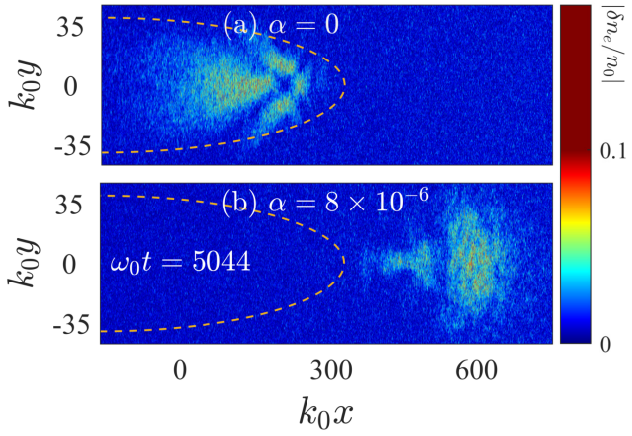

FIG. 14. The EPW amplitudes in $x-y$-space taken at $\omega_0 t = 5044$. The EPW is driven by the beating between a Gaussian pump laser and a counter-propagating seed wave. The cases without and with frequency chirp are indicated in the top and bottom panels, respectively. The envelopes of the laser speckles are represented by the yellow ellipses.

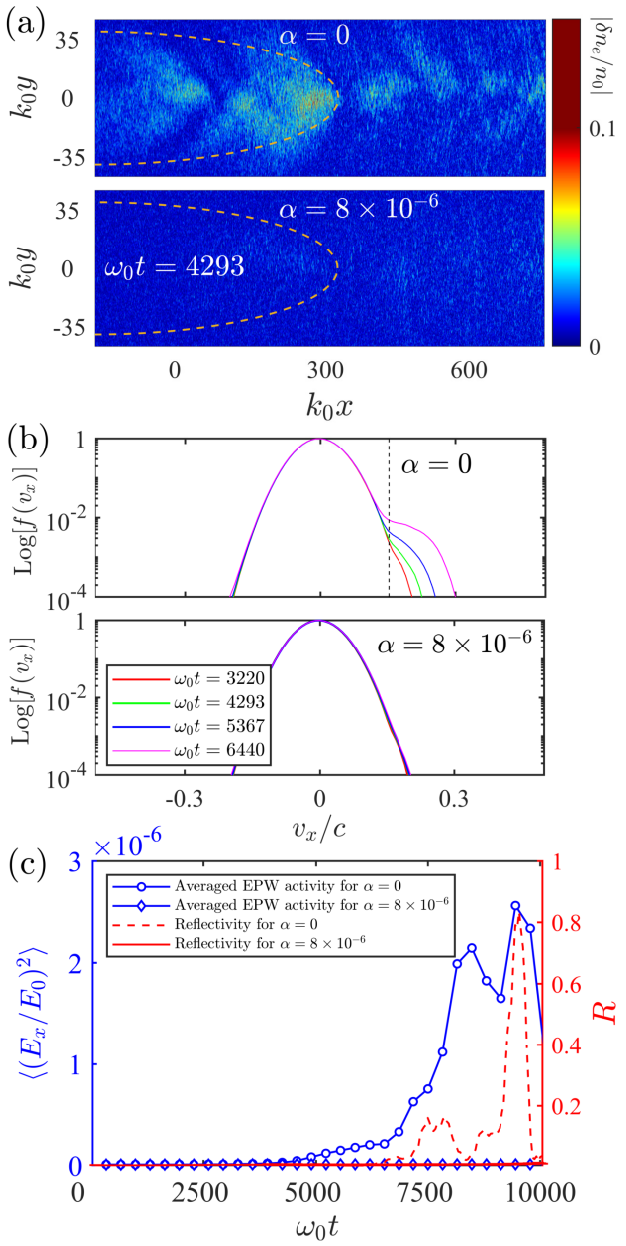

FIG. 15. 2D PIC simulation results of SRS with and without frequency chirp in the pump laser, where the SRS is seeded by the background noise in plasma. (a) Comparison of the contours in $x-y$-space of the EPW amplitude between the two cases without and with the frequency chirp ($\alpha = 8\times10^{-6}$) at $\omega_0 t = 4293$; (b) Electrons velocity distribution at a series of time instants; (c) Temporal evolution of $\langle |E_x|^2 \rangle$ for the averaged EPW activity (left axis) inside the domain $k_0 y \in [-35, 35]$, and SRS reflectivities (right axis).

In addition, the subsequent evolution of EPW at $\omega_0 t$ =5044 is recorded in Fig. 14. Without applying chirp, see top panel, the EPW evolves into a nonlinear stage where the autoresonance limit is reached. Self-focusing of the EPW occurs inside the speckle[63], suggesting strong excitation of EPW. In the bottom panel, where frequency chirp is applied, the EPW propagates up to a position far away from the speckle. The local laser intensity at this position is much lower than at speckle peak intensity. Since in our simulation case, the counter-propagating seed light is always injected, the ponderomotive force outside the speckle is still strong,

making the difference of EPW amplitudes between the two cases not much apparent. However, in realistic situations, SRS is only seeded by the background electron density fluctuations. The effect of frequency chirp on mitigating the scattering is much more significant than in the former case. For the case when the seed light field is switched off, Fig. 15(a) shows the EPW when comparing the cases without and with frequency chirp. The EPWs are obviously excited inside and outside the speckle in the case without a chirp. Furthermore, significant trapped-particle effects result in a plateau around the phase velocity (the vertical black dashed line) in the VDF of electrons, as indicated in the top panel of Fig. 15(b). This trapping effect leads to a nonlinear frequency shift and the reduced Landau damping of EPW. The inflationary growth of SRS[6] is expected as shown in Fig. 15(c). Meanwhile, hot electrons generated in an intense speckle can then potentially decrease the SRS threshold of the neighboring less-intense speckles as stated in Ref. 53. This has not been verified in our study where we have considered a single speckle.

By introducing a laser chirp rate with $\alpha = 8 \times 10^{-6} > \alpha_c$, the EPW initially excited inside the intense speckle moves quickly out of the speckle. Namely, the time $2\pi^2 F^2/v_{re}$ for which the EPW stays inside the speckle can be shorter than the interaction time. Thus the EPW propagates out of the speckle before it grows to a high level. As a result, no obvious EPW is excited as shown in the bottom panel of Fig. 15(a). Subsequently, no hot electrons are generated as shown in the bottom panel of Fig. 15(b). Meanwhile, the temporal evolution of $\langle |E_x|^2 \rangle$ or the averaged EPW activity inside the domain $k_0 y \in [-35, 35]$ is shown in Fig. 15(c) by the blue lines. This simulation shows again that a large laser frequency chirp rate can suppress the growth of EPW, and decrease the coupling between the EPW and the incident laser, then lead to strongly mitigated reflectivity, as shown by the red solid line in Fig. 15(c).

V. CONCLUSIONS AND DISCUSSION

We have presented a theoretical model to describe the effects of laser frequency chirp on SRS. It is based upon the governing equation for the EPW driven by the ponderomotive force due to the beating between the pump laser with a frequency chirp and the scattered light. The spatio-temporal evolution of the EPW is analyzed based on the governing equation. A propagation velocity v_{re} for the resonant EPW excitation is identified with Eq. (10), which results from the cancellation between the detuning brought by the frequency chirp and the resonance mismatch due to an inhomogeneous plasma density profile. It is found that the propagation of the central part of the EPW essentially follows the velocity v_{re}, which is the velocity with which the SRS resonance point in the plasma profile moves in the presence of a chirp. This motion with v_{re} can be faster than the group velocity of the EPW provided the chirp rate is larger than the critical value $\alpha_c = v_L^2 k^{'}/(1 - v_L)^2$. Particularly, in the kinetic regime, where the kinetic inflation occurs, the nonlinear kinetic effects can adjust this cancellation and modify the evolution of the EPW, which is well described by the solution Eq. (9). Also the impact of the frequency chirp on the phase-locking phenomenon associated with the EPW excitation is discussed. It is found that a negative frequency chirp rate can make the phase-locking area broader and thus promote the growth of the EPW and, subsequently, the growth of the SRS. However, a positive frequency chirp, especially for $\alpha > \alpha_c$, can destroy this phase-locking and thus suppress the instability. Note the dramatically different effects between the positive and negative frequency chirps on the SRS excitation even though their overall laser frequency spectra are the same.

One and two-dimensional kinetic PIC simulations have been carried out which reproduce the essential properties obtained from the envelope equation analysis. It is confirmed that for the chirp parameter $\alpha > \alpha_c$, the breaking of the phase-locking due to the frequency chirp not only suppresses the growth of EPW, but also mitigates the scattering reflectivity. Considering a single speckle in the two-dimensional configuration, it is found that the EPW initially driven inside the speckle can move quickly out of the zone of peak intensity for a proper choice of the chirp rate. In simulations with three-dimensional geometry we expect that the physics remains qualitatively very similar to the two-dimensional case, with a quantitative change concerning the lateral loss of escaping particles. By reducing the coupling between the EPW and the pump laser in this manner, the EPW amplitude, hot electron production, and scattering reflectivity are significantly mitigated as compared to the case without a frequency chirp.

Although only a single speckle is considered here, our study suggests a way to mitigate the kinetic inflationary growth by introducing frequency chirp in the pump laser with certain bandwidth values. In the case with multi-speckle laser beams, the EPWs excited inside several intense speckles generally would lead to kinetic inflationary scattering, and the hot electrons created in the speckles would result in reduced nonlinear Landau damping, indirectly decreasing the SRS threshold in the neighboring speckles[53,61,62]. As mentioned above, when a proper frequency chirp is introduced, the EPW excited in speckles may quickly leave the region of vigorous interaction before it grows to a high level. Subsequently, the EPW will experience the Landau damping after leaving the area, where the Landau damping would not be reduced due to the small production of hot electrons. This damping can then dissipate the EPW quickly. As a consequence, the EPW excited in a speckle has then a negligible influence on the neighboring speckles. Therefore, the local and global SRS scattering can be mitigated by introducing a proper frequency chirp.

Generally, beams with speckle structure due to optical

smoothing are used in the context of laser-plasma experiments, with pulse duration between a few ps and hundreds of ps. Experiments with a small number of speckles have been carried out in the past to study SRS also in the kinetic regime, based on relatively short pulses using chirp[64,65]. However, the available facility (ELFIE at the LULI facility) had certainly moderate chirp rates. For longer laser pulse duration, beyond tens of ps, relatively high chirp rates considered in our discussion above may also not be realistic.

Note that the speckles located at the different positions in the direction of laser propagation would encounter different central frequencies $1+\alpha t$, so that the SRS inside speckles from subsequent layers would be driven independently in inhomogeneous plasmas. Hence to mitigate the SRS inside different speckles, the condition of $\alpha > \alpha_c$ should be satisfied locally. The frequency shift arising during the time that the EPW needs to propagate through the speckle, i.e., from the center to the rear of the speckle, namely, $2\alpha\pi^2F^2/v_{re}$ should be not more than a few percent. This criterion limits the validity of our model.

Considering the recently reported experimental results in Ref. 2, SRS signatures have been observed from densities inferred to be near $n_{cr}/4$ and at lower densities (~ 0.15 to $0.21n_{cr}$, where n_{cr} is the critical density for laser wavelength $\lambda_0 = 0.351\mu m$), with the density scale lengths, $L = 400$ to 700μm, electron temperatures of T_e =3 to 5KeV and the focusing F-number of 8. In order to mitigate SRS for at least $10ps$ under these conditions, it is required that $\alpha > \alpha_c$ in every speckle, which corresponds to the minimum value of α is 3.5×10^{-6}. The frequency shift $2\alpha\pi^2F^2/v_{re}$ inside a speckle is then about 5%; the latter guarantees that our model and analysis in Sec. III can be applied in speckles under these parameter conditions. Meanwhile, in another experiment relevant for shock ignition[1], SRS was mainly driven in the electron density range between $0.03n_{cr}$ and $0.07n_{cr}$ (with n_{cr} for laser wavelength $\lambda_0 = 0.527\mu m$) with the density scale length $L = 400\mu$m, electron temperatures in the range of 1–1.2 keV, and focusing f-number of 2.5. To satisfy $\alpha > \alpha_c$ in speckles and mitigate SRS for at least $10ps$, the minimum value of α is 7.4×10^{-7}, with a frequency shift $2\alpha\pi^2F^2/v_{re}$ inside any speckle of about 0.3%. Both requirements are smaller than that in the former case by one order of magnitude.

Due to technological constraints in major laser facilities using Nd-glass lasers, the wavelength shift by chirp for a pulse duration of hundreds of ps can hardly exceed 1nm for 3ω, which means that the linear chirp rate α cannot be more than 5.3×10^{-9} for 3ω being by orders of magnitude below the requirements discussed above. For frequency doubled (2ω, 'green') Nd-glass laser light, using a technique with Nitrogen gas[66], the circumstances to achieve stronger wave length shifts seem to be more favorable since higher bandwidth values have been achieved, namely up to 8 THz.[67–69].

However, the results of our work can be applied to laser speckles of smoothed laser beams, as long as the laser pulse can contain several speckle layers, such that $c\,t_{pulse} \gtrsim L_{\rm beam}$ with a beam length typically determined by $L_{\rm beam} \sim M(F\lambda_0 L_\perp)^{1/2}$ with M as a numerical factor and $L_\perp$ ($\gg F\lambda_0$) denoting the total beam width.[70]

ACKNOWLEDGMENTS

The work was supported by the Strategic Priority Research Program of Chinese Academy of Sciences (Grant No. XDA25050100), the National Natural Science Foundation of China (Grant No. 11775144), the Science Challenge Project (No. TZ2018005), and the China Scholarship Council. This work has been carried out within the framework of the EUROfusion Consortium, funded by the European Union via the Euratom Research and Training Programme (Grant Agreement No 101052200 – EUROfusion). Views and opinions expressed are however those of the authors only and do not necessarily reflect those of the European Union or the European Commission. Neither the European Union nor the European Commission can be held responsible for them. The authors also thank Qing Wang, Zhao Liu, and Hanzhi Zhao, Gabriele Cristoforetti, R.H. Scott, and Denis Penninckx for useful discussions about the physics model and laser bandwidth issues as well as Jing Wang, Wanguo Zheng for helpful discussions about the laser technology.

AUTHOR DECLARATIONS

Conflict of Interest

The authors have no conflicts to disclose.

DATA AVAILABILITY

The data that support the findings of this study are available from the corresponding author upon reasonable request.

Appendix: Regarding the role of non-zero t_0 on EPW excitation

Eq. (9) is obtained by setting $x_0 = t_0 = 0$, for simplicity. Here we briefly discuss the effects of non-zero t_0 on EPW excitation, but still set $x_0 = 0$ without the loss of generality. The choice of non-zero t_0 means a non-zero initial phase $\psi = -\alpha t_0^2/2$ in the central plasma. In terms of frequency, non-zero t_0 values correspond to an initial frequency shift term $-\alpha t_0$ relative to the laser frequency ω_0, thus, we have a new initial laser frequency, $\omega_0' = 1-\alpha t_0$. We consider the complete phase carried by the laser field,

$$\theta = x - t - \alpha[x-(t-t_0)]^2/2, \tag{A.1}$$

Taking $k_0' = 1-\alpha t_0$, $\omega_0' = 1-\alpha t_0$, $\alpha' = \alpha(1/\omega_0')^2$ and $x' = k_0' x$, $t' = \omega_0' t$, one obtains

$$\begin{aligned}\theta &= (1-\alpha t_0)x - (1-\alpha t_0)t - \alpha[x-t]^2/2 - \alpha t_0^2/2,\\ &= x' - t' - \alpha'[x'-t']^2/2.\end{aligned}$$

The constant term $-\alpha t_0^2/2$ is dropped for not influencing the solution. Now the resulting chirp phase is $\psi' = -\alpha'(x' - t')^2/2$, which has the same form as Eq. (4) by taking $x_0 = t_0 = 0$. The latter we have adopted to perform our analysis in Sec. III. This confirms that taking $t_0 = 0$ for simplicity in Sec. III is reasonable and does not lose generality.

However, it is important to emphasize that the different values of t_0 matter when considering optically smoothed laser beams, which consist of numerous speckles. The speckles located at the different positions in the direction of laser propagation would encounter different t_0, thus the central frequencies of different speckles are $\omega_0' = 1 - \alpha t_0$, and the SRS inside different speckles layers may be driven independently. However, the SRS inside different speckles still follows the analysis and modeling in Sec. III, provided that SRS is in the kinetic regime.

REFERENCES

[1] G. Cristoforetti, S. Hüller, P. Koester, L. Antonelli, S. Atzeni, F. Baffigi, D. Batani, C. Baird, N. Booth, M. Galimberti, and et al., High Power Laser Science and Engineering **9**, e60 (2021).

[2] M. Rosenberg, A. Solodov, W. Seka, R. Follett, J. Myatt, A. Maximov, C. Ren, S. Cao, P. Michel, M. Hohenberger, *et al.*, Physics of Plasmas **27**, 042705 (2020).

[3] M. N. Rosenbluth, Physical Review Letters **29**, 565 (1972).

[4] T. Chapman, S. Hüller, P. E. Masson-Laborde, W. Rozmus, and D. Pesme, Physics of Plasmas **17**, 122317 (2010), https://doi.org/10.1063/1.3529362.

[5] T. Chapman, S. Hüller, P. E. Masson-Laborde, A. Heron, D. Pesme, and W. Rozmus, Phys Rev Lett **108**, 145003 (2012).

[6] S. J. Spencer, A. G. Seaton, T. Goffrey, and T. D. Arber, Physics of Plasmas **27**, 122705 (2020), https://doi.org/10.1063/5.0022901.

[7] M. Luo, S. Hüller, M. Chen, and Z. Sheng, Physics of Plasmas **29**, 032102 (2022), https://doi.org/10.1063/5.0078985.

[8] J. J. Thomson and J. I. Karush, The Physics of Fluids **17**, 1608 (1974), https://aip.scitation.org/doi/pdf/10.1063/1.1694940.

[9] G. Laval, R. Pellat, D. Pesme, A. Ramani, M. N. Rosenbluth, and E. A. Williams, The Physics of Fluids **20**, 2049 (1977), https://aip.scitation.org/doi/pdf/10.1063/1.861824.

[10] W. Kruer, *The physics of laser plasma interactions* (crc Press, 2019).

[11] D. Eimerl and A. J. Schmitt, Plasma Physics and Controlled Fusion **58**, 115006 (2016).

[12] A. Fusaro, P. Loiseau, D. Penninckx, G. Riazuelo, and R. Collin, Nuclear Fusion **61**, 126049 (2021).

[13] R. K. Follett, J. G. Shaw, J. F. Myatt, C. Dorrer, D. H. Froula, and J. P. Palastro, Physics of Plasmas **26**, 062111 (2019), https://doi.org/10.1063/1.5098479.

[14] R. K. Follett, J. G. Shaw, J. F. Myatt, H. Wen, D. H. Froula, and J. P. Palastro, Physics of Plasmas **28**, 032103 (2021).

[15] Y. Zhao, S. Weng, M. Chen, J. Zheng, H. Zhuo, C. Ren, Z. Sheng, and J. Zhang, Physics of Plasmas **24**, 112102 (2017), https://doi.org/10.1063/1.5003420.

[16] S. Skupsky, R. W. Short, T. Kessler, R. S. Craxton, S. Letzring, and J. M. Soures, J. Appl. Phys. **66**, 3456 (1989).

[17] J. E. Rothenberg, J. Opt. Soc. Am. B **14**, 1664 (1997).

[18] J. Garnier, L. Videau, C. Gouédard, and A. Migus, J. Opt. Soc. Am. A **14**, 1928 (1997).

[19] J. E. Rothenberg, Journal of Applied Physics **87**, 3654 (2000), https://doi.org/10.1063/1.372395.

[20] E. Lefebvre, R. L. Berger, A. B. Langdon, B. J. MacGowan, J. E. Rothenberg, and E. A. Williams, Physics of Plasmas **5**, 2701 (1998), https://doi.org/10.1063/1.872957.

[21] S. Hüller, P. Mounaix, and V. T. Tikhonchuk, Physics of Plasmas **5**, 2706 (1998), https://doi.org/10.1063/1.872958.

[22] H. H. Ma, X. F. Li, S. M. Weng, S. H. Yew, S. Kawata, P. Gibbon, Z. M. Sheng, and J. Zhang, Matter and Radiation at Extremes **6**, 055902 (2021), https://doi.org/10.1063/5.0054653.

[23] H. Wen, R. K. Follett, A. V. Maximov, D. H. Froula, F. S. Tsung, and J. P. Palastro, Physics of Plasmas **28**, 145003 (2021).

[24] P. N. Guzdar, C. S. Liu, and R. H. Lehmberg, Physics of Fluids B: Plasma Physics **3**, 2882 (1991).

[25] J. Garnier, Phys. Plasmas **6**, 1601 (1999).

[26] D. A. Russell, D. F. DuBois, and H. A. Rose, Physics of Plasmas **6**, 1294 (1999).

[27] L. Yin, B. J. Albright, H. A. Rose, K. J. Bowers, B. Bergen, D. S. Montgomery, J. L. Kline, and J. C. Fernández, Physics of Plasmas **16**, 113101 (2009).

[28] L. Yin, B. J. Albright, H. A. Rose, D. S. Montgomery, J. L. Kline, R. K. Kirkwood, P. Michel, K. J. Bowers, and B. Bergen, Physics of Plasmas **20**, 012702 (2013).

[29] D. Strickland and G. Mourou, Optics Communications **55**, 447 (1985).

[30] R. Nuter and V. Tikhonchuk, Phys. Rev. E **87**, 043109 (2013).

[31] B. Ersfeld and D. A. Jaroszynski, Phys. Rev. Lett. **95**, 165002 (2005).

[32] G. Vieux, A. Lyachev, X. Yang, B. Ersfeld, J. P. Farmer, E. Brunetti, R. C. Issac, G. Raj, G. H. Welsh, S. M. Wiggins, and D. A. Jaroszynski, New Journal of Physics **13**, 063042 (2011).

[33] V. M. Malkin, G. Shvets, and N. J. Fisch, Phys. Rev. Lett. **84**, 1208 (2000).

[34] F. Amiranoff, C. Riconda, M. Chiaramello, L. Lancia, J. R. Marquès, and S. Weber, Physics of Plasmas **25**, 013114 (2018), https://doi.org/10.1063/1.5019374.

[35] M. Chiaramello, F. Amiranoff, C. Riconda, and S. Weber, Phys Rev Lett **117**, 235003 (2016).

[36] S. Hüller, P. Mulser, and A. M. Rubenchik, Phys. Fluids B **3**, 3339 (1991), https://doi.org/10.1063/1.859994.

[37] L. Friedland and A. Shagalov, Physical Review E **89**, 053103 (2014).

[38] L. Friedland, G. Marcus, J. Wurtele, and P. Michel, Physics of Plasmas **26**, 092109 (2019).

[39] P. Khain and L. Friedland, Physics of Plasmas **14**, 082110 (2007), https://doi.org/10.1063/1.2771515.

[40] P. Khain and L. Friedland, Physics of Plasmas **17**, 102308 (2010), https://doi.org/10.1063/1.3500246.

[41] J. Faure, J.-R. Marquès, V. Malka, F. Amiranoff, Z. Najmudin, B. Walton, J.-P. Rousseau, S. Ranc, A. Solodov, and P. Mora, Phys. Rev. E **63**, 065401 (2001).

[42] T.-W. Yau, C.-J. Hsu, H.-H. Chu, Y.-H. Chen, C.-H. Lee, J. Wang, and S.-Y. Chen, Physics of Plasmas **9**, 391 (2002), https://doi.org/10.1063/1.1430251.

[43] C. B. Schroeder, E. Esarey, B. A. Shadwick, and W. P. Leemans, Physics of Plasmas **10**, 285 (2003), https://doi.org/10.1063/1.1528901.

[44] S. Baton, A. Colaïtis, C. Rousseaux, G. Boutoux, S. Brygoo, L. Jacquet, M. Koenig, D. Batani, A. Casner, E. L. Bel, D. Raffestin, A. Tentori, V. Tikhonchuk, J. Trela, C. Reverdin, L. Le-Deroff, W. Theobald, G. Cristoforetti, L. Gizzi, P. Koester, L. Labate, and K. Shigemori, High Energy Density Physics **36**, 100796 (2020).

[45] D. S. Montgomery, J. A. Cobble, J. C. Fernández, R. J. Focia, R. P. Johnson, N. Renard-LeGalloudec, H. A. Rose, and D. A. Russell, Physics of Plasmas **9**, 2311 (2002), https://doi.org/10.1063/1.1468857.

[46] D. W. Forslund, J. M. Kindel, and E. L. Lindman, The Physics of Fluids **18**, 1002 (1975), https://aip.scitation.org/doi/pdf/10.1063/1.861248.

[47] J. L. Kline, D. S. Montgomery, L. Yin, D. F. DuBois, B. J. Albright, B. Bezzerides, J. A. Cobble, E. S. Dodd, D. F. DuBois, J. C. Fernández, R. P. Johnson, J. M. Kindel, H. A. Rose, H. X.

Vu, and W. Daughton, Physics of Plasmas **13**, 055906 (2006), https://doi.org/10.1063/1.2178777.
[48]To the second harmonic, it gives $\zeta = 15v_{th}^2c^2\omega_L^3/(4v_\phi^4\omega_{pe}^2)$, where $v_\phi = \omega_L/k_L$ is the phase velocity of EPW.
[49]T. P. Coffey, The Physics of Fluids **14**, 1402 (1971), https://aip.scitation.org/doi/pdf/10.1063/1.1693620.
[50]R. L. Dewar and J. Lindl, The Physics of Fluids **15**, 820 (1972), https://aip.scitation.org/doi/pdf/10.1063/1.1693990.
[51]B. J. Winjum, J. Fahlen, and W. B. Mori, Physics of Plasmas **14**, 102104 (2007), https://doi.org/10.1063/1.2790385.
[52]G. J. Morales and T. M. O'Neil, Physical Review Letters **28**, 417 (1972).
[53]B. J. Winjum, A. Tableman, F. S. Tsung, and W. B. Mori, Physics of Plasmas **26**, 112701 (2019), https://doi.org/10.1063/1.5110513.
[54]O. Yaakobi, L. Friedland, R. R. Lindberg, A. E. Charman, G. Penn, and J. S. Wurtele, Physics of Plasmas **15**, 032105 (2008), https://doi.org/10.1063/1.2884717.
[55]T. Chapman, *Autoresonance in Stimulated Raman Scattering*, Doctoral thesis, Ecole Polytechnique, Palaiseau, France (2011).
[56]J. Fajans, E. Gilson, and L. Friedland, Physics of Plasmas **6**, 4497 (1999).
[57]J. Fajans, E. Gilson, and L. Friedland, Physics of Plasmas **8**, 423 (2001).
[58]T. D. Arber, K. Bennett, C. S. Brady, A. Lawrence-Douglas, M. G. Ramsay, N. J. Sircombe, P. Gillies, R. G. Evans, H. Schmitz, A. R. Bell, and C. P. Ridgers, Plasma Physics and Controlled Fusion **57**, 113001 (2015).
[59]P. Michel, L. Divol, D. Turnbull, and J. D. Moody, Phys Rev Lett **113**, 205001 (2014).
[60]P. Michel, E. Kur, M. Lazarow, T. Chapman, L. Divol, and J. S. Wurtele, Phys. Rev. X **10**, 021039 (2020).
[61]L. Yin, B. J. Albright, H. A. Rose, K. J. Bowers, B. Bergen, R. K. Kirkwood, D. E. Hinkel, A. B. Langdon, P. Michel, D. S. Montgomery, and J. L. Kline, Physics of Plasmas **19**, 056304 (2012), https://doi.org/10.1063/1.3694673.
[62]L. Yin, B. J. Albright, H. A. Rose, D. S. Montgomery, J. L. Kline, R. K. Kirkwood, P. Michel, K. J. Bowers, and B. Bergen, Physics of Plasmas **20**, 012702 (2013), https://doi.org/10.1063/1.4774964.
[63]G. Tran, P. Loiseau, A. Fusaro, A. Héron, S. Hüller, L. Maëder, P.-E. Masson-Laborde, D. Penninckx, and G. Riazuelo, Physics of Plasmas **27**, 122707 (2020), https://doi.org/10.1063/5.0018669.
[64]C. Rousseaux, K. Glize, S. D. Baton, L. Lancia, D. Bénisti, and L. Gremillet, Phys. Rev. Lett. **117**, 015002 (2016).
[65]K. Glize, C. Rousseaux, D. Bénisti, V. Dervieux, L. Gremillet, S. D. Baton, and L. Lancia, Physics of Plasmas **24**, 032708 (2017), https://doi.org/10.1063/1.4978879.
[66]The technique based on the use of Nitrogen gas may however have other limitations, namely on the beam quality in the near field. Personal communication with Denis Penninckx.
[67]D. Eimerl, D. Milam, and J. Yu, Phys. Rev. Lett. **70**, 2738 (1993).
[68]J. W. Bates, J. F. Myatt, J. G. Shaw, R. K. Follett, J. L. Weaver, R. H. Lehmberg, and S. P. Obenschain, Phys. Rev. E **97**, 061202 (2018).
[69]D. C. Wilson, M. L. Spaeth, L. Yin, J. P. Sauppe, L. B. Hopkins, E. N. Loomis, R. F. Sacks, B. J. Albright, D. Strozzi, D. Munro, C. Widmayer, B. Raymond, K. Manes, and J. L. Kline, Physics of Plasmas **28**, 052704 (2021), https://doi.org/10.1063/5.0037338.
[70]E.g., for $L_\perp = 100F\lambda_0$, with $F/8$, assuming $M \simeq 5$, the time $L_{\rm beam}/c$ would be of the order of $10ps \times(\lambda_0/\mu m)$.